A Low-cost GNSS/IMU/Visual monoSLAM/WSS Integration Based on Federated Kalman Filtering for Navigation in Urban Environments

Amani Ben Afia, Anne-Christine Escher, Christophe Macabiau

A Low-cost GNSS/IMU/Visual monoSLAM/WSS Integration Based on Kalman Filtering for Navigation in Urban Environments

Amani BEN AFIA, Anne-Christine ESCHER, Christophe MACABIAU
ENAC Telecom Lab, France

BIOGRAPHIES

Amani BEN AFIA graduated in 2012 as an Electronics engineer from ENAC (French National Civil Aviation School), Toulouse, France. Since 2013, she has been a PhD student in the Signal Processing and Navigation Research Group (SIGNAV) of ENAC. Her research focuses on developing multi-sensor fusion algorithms for the navigation in constrained environments.

Dr. Anne-Christine ESCHER graduated as an electronics engineer in 1999 from the ENAC in Toulouse, France. Since 2002, she has been working as a researcher and as a lecturer in the signal processing and navigation research group (SIGNAV) of the TELECOM Lab in the ENAC. She received her Ph.D. in 2003.

Dr. Christophe MACABIAU graduated as an electronics engineer in 1992 from the ENAC in Toulouse, France. Since 1994, he has been working on the application of satellite navigation techniques to civil aviation. He received his PhD in 1997 and has been in charge of the signal processing lab of ENAC since 2000.

ABSTRACT

Car navigation performance improvement is a subject of great interest nowadays especially with the development of autonomous car navigation. In urban environments, it is often difficult to rely on standalone *Global Navigation Satellite System* (GNSS) to obtain continuously an accurate and reliable navigation solution. In fact, the presence of buildings and other structures hindering the reception of GNSS signals (blockage, multipath, NLOS, poor geometry, etc.) makes it difficult for GNSS to provide accurate, continuous and reliable navigation solution in such an environment. A possible solution for this problem is to fuse information from a limited number of GNSS measurements and other sensors in order to enhance the system performance in terms of accuracy and availability. In this paper, we propose an integrated navigation system that fuses different sensor information in order to improve the car navigation performance in urban environments. A Low-cost navigation solution is proposed since the intended application is cost-sensitive. The proposed solution integrates information from an *Inertial Measurement Unit* (IMU), a GNSS receiver, a Wheel Speed Sensor (WSS) and a vision module based on monocular *Simultaneous Localization And Mapping* (SLAM). Motion constraints related to the movement of a land vehicle on the ground are also taken into account.

INTRODUCTION

The requirements in terms of navigation accuracy, integrity, continuity and availability are increasing for land vehicles especially with the development of autonomous land vehicles. In this work, the targeted 95% accuracy is of **1m** for the horizontal position and of **1°** for the attitude. These requirements are set by a French project called MIMOSA aiming to develop a low-cost navigation equipment for land vehicles capable of providing continuously an accurate navigation solution. One of the targeted applications of this project is the positioning of the garbage trucks in urban environments.

In the last decades, GNSS has been the most widely used system for navigation especially with its decreasing cost over the years. However, despite of its capability to provide absolute navigation information with long time accuracy, this system suffers from the problems related to signal propagation especially in urban environments where buildings, trees and other structures hinder the reception of GNSS signals. In addition to nominal errors, GNSS measurements suffer in urban environments from blockage reducing the number of satellites in view and resulting either in poor geometry degrading the navigation performance, or even in the unavailability of GNSS if the number of satellites of view is less than 4. The problem of unavailability will be handled in the near future with the development of new constellations such as GALILEO, BEIDOU, etc. The most important issue in urban environments is signal reflections which result in significant positioning error. When the *Line-Of-Sight* (LOS) signal is reflected and received with the reflected signal, this is known as *multipath*. If the LOS signal is blocked and only its reflection arrives to the receiver antenna, this is known as *Non-Line-Of-Sight* (NLOS) signal. The latter error results in a positive pseudo-range measurement error equal to the additional path delay and its value may exceed in some cases a kilometer [1]. Many techniques are proposed in the literature in order to mitigate these problems and improve the GNSS accuracy [1]. Unfortunately, all these techniques have limitations as highlighted in [1].

A possible way to overcome these problems is to fuse the "good" GNSS measurements with other sensors having complementary advantages. In fact, by exploiting the complementarity of sensors, hybridization algorithms can improve the navigation solution compared to solutions provided by each stand-alone sensor.

Generally, the most widely implemented hybridization algorithms for land vehicles fuse GNSS measurements with inertial and/or odometric data [2] [3]. Thereby, these *Dead-Reckoning* (DR) sensors ensure the system continuity when GNSS information is unavailable and improve the system performance when GNSS signals are corrupted, and in return the GNSS limits the drift of the DR solution if it is available. However the performance achieved by this hybridization depends thoroughly on the quality of the DR sensor used especially when GNSS signals are degraded or unavailable.

Since the targeted application is cost-sensitive and low-cost sensors should be used, the common solution of fusing GNSS with inertial and/or odometric data mentioned previously cannot provide the high performance required by the project. For this reason, the SLAM is proposed as an additional sensor having the potential to improve the navigation performance. In fact, cameras have become one of the most attractive positioning sensors in the last decades and it has been proven that vision techniques are capable of providing accurate navigation solution [4] while having reasonable cost. In general, vision systems reach very accurate results when using stereovision. However, the main drawback of such a configuration compared to a single camera is that in large-scale environments such as streets, the images captured by the cameras might contain objects that are placed too far. Processing these images does not allow recovering the depth values unless the stereo camera baseline is of few meters [5]. In addition to this compactness issue, a calibration issue arises when a multi-camera system is used and the calibration of a single camera is much easier [6]. Therefore, a single camera will be considered in this study. Nonetheless, in case of a monocular vision module, a classical issue due to the projective nature of a single camera arises: the depth information of a 3D world point projected onto the image plane cannot be recovered using a single camera since a single 2D image point is the projection of an infinite number of 3D world points. This depth ambiguity results in a scale factor affecting the position estimated by the visual module and decreases dramatically its accuracy. Therefore, the visual navigation solution accuracy depends thoroughly on the good estimation of this scale factor. However the attitude estimation using a monocular camera is free from scale. This latter visual information is very important especially with the use of low-cost inertial sensors with bad gyroscope quality. In order to estimate this information, a vision module based on monocular SLAM technique is used as a black box providing the attitude. A review of SLAM algorithm is performed in [7]. Compared to simple visual odometry, this technique has the advantage of reducing the estimation error using the bundle adjustment process described in [8]. In this study, only the visual heading provided by the SLAM is used since we focus on horizontal navigation performance.

In addition to the low-cost sensors mentioned above, motion constraints for land vehicles are costless solutions capable of improving navigation performance. These constraints consist of *Non-Holonomic-Constraints* (NHC) [9], *Zero Velocity Update* (ZVU) [10] and *Zero Angular Rate Update* (ZARU) [10]. NHC assume that the vehicle does not move in the plane perpendicular to the forward direction. ZVU and ZARU are applied when the navigation system is stationary. They respectively constrain the vehicle velocity and angular rate to be equal to zero when a stationarity is detected. When GNSS is unavailable or corrupted, this information helps reducing the navigation solution drift.

The work proposed in this paper takes advantage of all the low-cost possible ways to improve the navigation solution mentioned above and uses their information in an integrated multi-sensor system. In the proposed architecture, the *Inertial Navigation System* (INS) is selected as the reference sensor since it provides a complete and continuous navigation solution including position, velocity and attitude with the highest rate. The INS estimation errors are corrected by GNSS, vision, WSS and motion constraints measurements using an error-state EKF based on a closed loop configuration. When GNSS measurements (pseudo-ranges and Doppler) are available, an innovation test [10] checking the consistency of new measurements with previous information is applied in order to exclude measurements considered as corrupted. When GNSS is unavailable, the filter keeps on running with the other measurements. Since the GNSS measurements have the lowest rate and are not necessarily available, this architecture is such as a virtual DR sensor is running continuously using the inertial, visual, odometric and motion constraints measurements. When GNSS measurements arrive, they allow the calibration of the DR system, otherwise the DR system works continuously without having a large drift.

The paper is organized as follows. First the notations and coordinate frames used are described. Second, the integrated navigation system is detailed and the fusion strategy is proposed. The equations of the process and measurement models are presented and discussed. Then, the performance analysis of the proposed algorithm is performed. Finally, conclusions are given at the end the paper.

COORDINATE FRAMES AND NOTATIONS

Before tackling the sensor fusion strategy, it is important to remind the different coordinate frames associated to the sensors and the relationship between them.

Figure 1 illustrates the coordinate frames we use: we assume that the IMU platform and the vehicle body frame (*b*) are aligned. This frame is attached to the vehicle center of gravity. Its X-axis points towards the right side

of the vehicle, its Y-axis points towards the forward direction and its Z-axis points upwards and completes the right handed frame. The local frame (l) is defined by the *East North Up* (ENU) local tangent plane. This frame is attached to a local point (the initial navigation point is chosen in our study), and its X, Y and Z axis point towards the east, north and up directions, respectively. The Earth-Centered-Earth-Fixed frame (E) is attached to the Earth center of mass. Its X-axis points towards the intersection between the prime meridian and the equator plane, its Z-axis extends through the Earth spin axis and its Y-axis completes the right handed coordinate system. The geodetic coordinates (latitude, longitude and altitude) are defined with respect to this coordinate system. The vision frame (v) is the frame in which the SLAM provides its outputs. This frame is attached to the initial pose of the vehicle [11] and is defined up to rotation with respect to the (l) frame. If we assume that the IMU and the camera are aligned, then this rotation corresponds to the initial (b) to (l) rotation.

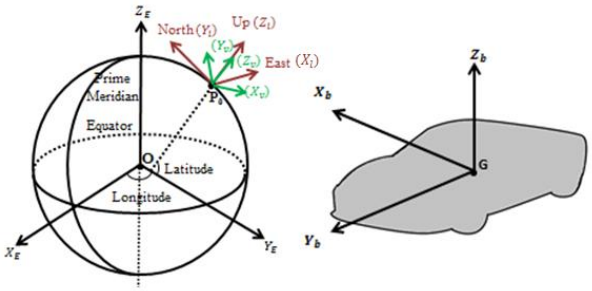

Figure 1: Reference frames

In this paper, the notations with the hat, ^, are the estimated quantities and those with the tilde, ~, are the measured quantities. The notations without hat or tilde are the actual quantities.

We assume that all the lever arms and orientation between the aiding sensors and the IMU are perfectly known and are measured before the navigation starts. Let us note:
- $\Delta \boldsymbol{p}_G^b$ the lever arm between GPS antenna and IMU:
- $\Delta \boldsymbol{p}_w^b$ the lever arm between the center of the rear axle of the vehicle and IMU:

Table 1 specifies, for each sensor, the outputs and the associated coordinate system.

Nav. module	Output		Frame	Frame Origin
INS	INS Position	$\widehat{\boldsymbol{p}}_b^l$	(l)	Initial vehicle position
	INS Velocity	$\widehat{\boldsymbol{v}}_b^l$		
	INS Attitude	$\widehat{\boldsymbol{C}}_{b2l}$		
GNSS	ith Pseudo-range	$\tilde{\rho}_G^i$	--	--
	ith Doppler	$\tilde{d}_G^i$		
VSLAM	Camera heading	$\tilde{\psi}_{SLAM}$	(v)	Initial vehicle position
WSS	Velocity	$\tilde{v}_w^{by}$	(b)	Vehicle center of mass

Table 1: Sensor outputs

NAVIGATION FILTER

Multi-sensor system design

The aim of this study is to develop a low-cost multi-sensor fusion system capable of providing accurate navigation information for land vehicles in urban environments. The proposed architecture consists of a single frequency GNSS receiver providing pseudo-range and Doppler measurements for each satellite in view, a low-cost IMU, a vision module processing the images of a single camera using the SLAM technique and providing heading information, a WSS providing the vehicle velocity and constraints describing the motion of the vehicle. The IMU is selected as the reference sensor since it is the only sensor continuously providing a complete navigation solution (position, velocity and attitude) at the highest rate. The mechanization providing these quantities is implemented in the (l) frame. As shown in **Figure 2**, the INS mechanization errors are corrected by the measurements of the other sensors. An error-state EKF is used in order to estimate the corrections that should be applied to the inertial navigation solution. As highlighted in [2] and [12], it is preferred to express the position error in meters than in radians in order to avoid numeric instability inside the filter. Hence, the (l) frame is used as the reference system instead of geodetic coordinates. The estimated IMU measurement errors (biases and scale factors) are fed back to the mechanization since we have to deal with a low-cost IMU. Otherwise the mechanization can experience unbounded error growth, and the assumption of small errors used in the linearization process of the filter can be violated [2]. WSS measurement is affected by an unknown scale factor due to the tire radius change. This scale factor should be estimated and the WSS velocity should be corrected in order to obtain a good velocity measurement used to update the Kalman filter. Since the WSS provides only the forward velocity (along Y_b), the NHC completes the three-dimensional velocity by assuming that for a ground vehicle, the lateral and vertical velocities (along X_b and Z_b) should be equal to zero if the vehicle does not slip or jump.

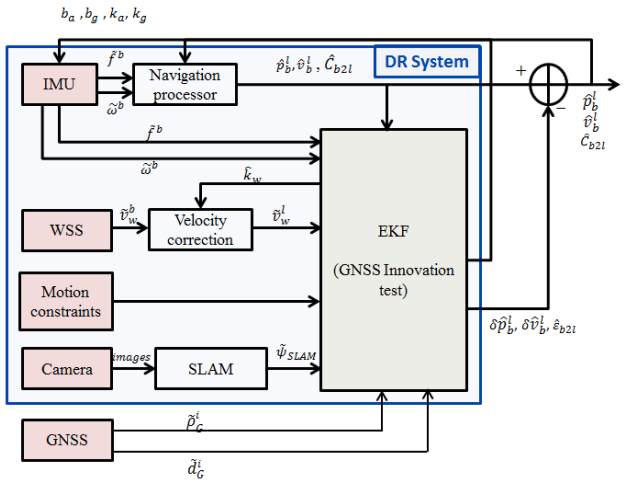

Figure 2: Filter architecture

The ZVU is used when a stationarity is detected. This detection is based on the comparison of the WSS velocity mean with a threshold over a suitable time window. Normally, the ZVU is useless in the presence of the WSS and NHC. However, the assumption of no side slip of the NHC could be violated in practical situations. To avoid NHC violations, NHC is modelled as:

$$v_{xb} = \eta_{xb} \quad \textbf{(1)}$$

$$v_{zb} = \eta_{zb} \quad \textbf{(2)}$$

where η_{xb} and η_{zb} are Gaussian white noise sources with zero mean and a relatively high standard deviation equal to 0.5 m/s [12]. When a stationarity is detected, the trust that we have in a zero velocity increases and the standard deviation associated to the velocity measurement can be decreased. We set this standard deviation to **0.01 m/s**.
The ZARU is also applied in vehicle stationarity. It is also applied when a linear motion is detected. This detection is performed by comparing the standard deviation of the yaw rate obtained from differential odometry with a threshold or by using the steering angle information if available.

The idea of using visual, odometric and motion constraints measurements to correct the inertial sensor is to form a DR system running without interruption. This system is capable of remarkably reduce the drift compared to a stand-alone running inertial system.

As discussed in the introduction, GNSS measurements, if available, are very likely to be corrupted by reflections and blockage. Therefore, measurements affected by large errors should be detected and removed to avoid the degradation of the navigation solution. This detection is performed by an innovation test [10] that compares the normalized Kalman filter innovation to a threshold and removes measurements that are not consistent with previous information. The remaining measurements are used to update the filter with absolute information. If GNSS is not available, then the DR system keeps on running to ensure the navigation continuity.

Inertial Sensor Model
An IMU is at least composed of accelerometers and gyroscopes. The accelerometers measure the specific force and the gyroscopes measure the angular rate. The measurements are provided in the body frame. In this work, 3 accelerometers and 3 gyroscopes are used. These measurements are inevitably affected by errors. For a low-cost IMU, these errors mainly consist of biases, scale factors and noise [12]. In this study, the inertial measurements are modelled by the following equations:

$$\tilde{\boldsymbol{f}}^b = (\boldsymbol{I_3} + \boldsymbol{k}_a) \cdot \boldsymbol{f}^b + \boldsymbol{b}_a + \boldsymbol{\eta}_a \quad \textbf{(3)}$$

$$\tilde{\boldsymbol{\omega}}^b = \left(\boldsymbol{I_3} + \boldsymbol{k}_g\right) \cdot \boldsymbol{\omega}^b + \boldsymbol{b}_g + \boldsymbol{\eta}_g \quad \textbf{(4)}$$

where $\tilde{\boldsymbol{f}}^b$ and $\tilde{\boldsymbol{\omega}}^b$ are respectively the measured specific force and angular rate in the body frame. $\boldsymbol{f}^b$ and $\boldsymbol{\omega}^b$ are the actual specific force and angular rate. $\boldsymbol{k}_a$ and $\boldsymbol{k}_g$ are the scale factors. $\boldsymbol{b}_a$ and $\boldsymbol{b}_g$ are the biases, and $\boldsymbol{\eta}_a$ and $\boldsymbol{\eta}_g$ are zero-mean white Gaussian noises.

GNSS measurement model
The code pseudo-range measurement is the distance between the GNSS satellite and the receiver antenna. This measurement is computed from the propagation time between the transmission of the signal by the satellite and its reception by the receiver, and the multiplication of this time by the speed of light c. The fact that the clocks of the satellites and the receiver are not perfectly synchronized to GPS time, introduces a clock bias that drifts within time. Therefore, the pseudo-range measurement can be modeled as:

$$\tilde{\rho}_G^i = r^i + c\delta t_0 + \eta_{\rho G}^i \quad \textbf{(5)}$$

where r^i is the true range between the satellite i and the receiver antenna, δt_0 is the clock bias and $\eta_{\rho G}^i$ is a zero-mean white Gaussian noise modeling the residual of all nominal errors after correction.

The Doppler measurement represents the rate of change of the carrier phase. The multiplication of this measurement by the signal wavelength λ_0 provides the pseudo-range rate measurement:

$$\dot{\rho}_G^i = \tilde{d}_G^i . \lambda_0 = \dot{r}^i + c\dot{\delta} t_0 + \eta_{\dot{\rho} G}^i \quad \textbf{(6)}$$

where $\tilde{d}_G^i$ is the Doppler measurement of satellite i, $\dot{r}^i$ is the true pseudo-range rate between the satellite and the receiver, $\dot{\delta} t_0$ is the clock drift and $\eta_{\dot{\rho} G}^i$ is the range rate error modeled as a zero-mean Gaussian white noise.

WSS and NHC measurement model
WSS provides velocity along the forward axis in the (b) frame. The measurement model of the WSS is given in by:

$$\tilde{\boldsymbol{v}}_w^l = \boldsymbol{C}_{b2l}(1 + k_w)\tilde{\boldsymbol{v}}_w^b + \boldsymbol{\eta}_w \quad \textbf{(7)}$$

with $\tilde{\boldsymbol{v}}_w^b = \begin{bmatrix} 0 & \tilde{v}_w^{by} & 0 \end{bmatrix}^T$, k_w is the WSS scale factor and $\boldsymbol{\eta}_w$ is the WSS noise modeled as zero-mean, white and Gaussian. The lateral and vertical velocities are set to zero by taking into account the NHC.

Vision heading measurement model
This heading measurement is provided in the vision frame. This means that the vision module assumes that the initial heading of the vehicle is equal to zero. In order to obtain the heading of the vehicle with respect to the local frame $\tilde{\psi}_{SLAM}^l$, it should be corrected with the initial heading ψ_0^l:

$$\tilde{\psi}_{SLAM}^l = \tilde{\psi}_{SLAM}^v + \psi_0^l + \eta_\psi \quad \textbf{(8)}$$

where η_ψ is a Gaussian white noise. Note that this assumption only holds if the vehicle performs a loop

closure (the end of its trajectory is the starting point). In fact, by detecting again the same features, the SLAM is capable of eliminating the drift using the bundle adjustment process. If no loop closure is done, this assumption holds if the SLAM is aided by a previously built georeferenced database. If none of these two conditions is fulfilled, then the assumption of Gaussian white noise is not realistic for the heading measurement but holds for the estimated vehicle heading change between two images. Therefore the heading should be modeled as a random walk. The latter case will be studied in future works.

Sate Vector

The INS estimates the navigation parameters *i.e.* the position, velocity and attitude of the vehicle, and the aiding sensors correct the INS estimation error through the Kalman filter. The errors of the navigation parameters are defined by:

$$\delta \boldsymbol{p}_b^l = \widehat{\boldsymbol{p}}_b^l - \boldsymbol{p}_b^l \quad \textbf{(9)}$$

$$\delta \boldsymbol{v}_b^l = \widehat{\boldsymbol{v}}_b^l - \boldsymbol{v}_b^l \quad \textbf{(10)}$$

$$\widehat{\boldsymbol{C}}_{b2l} = (\boldsymbol{I} - \boldsymbol{E}_{b2l})\, \boldsymbol{C}_{b2l} \quad \textbf{(11)}$$

where $\boldsymbol{E}_{b2l}$ is the skew-symmetric matrix of the attitude error $\boldsymbol{\varepsilon}_{b2l} = [\varepsilon_E \quad \varepsilon_N \quad \varepsilon_U]$

Using the previous notations, a 21-element error state vector associated to INS is consequently used:

$$\delta \boldsymbol{x}_{INS} = \left[\delta \boldsymbol{p}_b^l \quad \delta \boldsymbol{v}_b^l \quad \boldsymbol{\varepsilon}_{b2l} \quad \delta \boldsymbol{b}_a \quad \delta \boldsymbol{b}_g \quad \delta \boldsymbol{k}_a \quad \delta \boldsymbol{k}_g\right]^T \quad \textbf{(12)}$$

Since WSS velocity is affected by an unknown scale factor, and GNSS clock bias and clock drift are also unknown, these quantities should be estimated by the filter. Therefore:

$$\delta \boldsymbol{x}_G = \left[\delta(c\delta t_0) \quad \delta\left(c\dot{\delta} t_0\right)\right]^T \quad \textbf{(13)}$$

$$\delta x_w = \delta k_w \quad \textbf{(14)}$$

The full EKF state is the concatenation of the state vectors associated to each sensor. It is given by the 24-element state vector:

$$\delta \boldsymbol{x} = [\delta \boldsymbol{x}_{INS}{}^T \quad \delta \boldsymbol{x}_G{}^T \quad \delta x_w]^T \quad \textbf{(15)}$$

State transition model

The INS mechanization equation is given by:

$$\begin{bmatrix} \dot{\boldsymbol{p}}_b^l \\ \dot{\boldsymbol{v}}_b^l \\ \dot{\boldsymbol{C}}_{b2l} \end{bmatrix} = \begin{bmatrix} \boldsymbol{v}_b^l \\ \boldsymbol{C}_{b2l}\boldsymbol{f}^b - \left(2\boldsymbol{\omega}_{ie}^l + \boldsymbol{\omega}_{el}^l\right) \times \boldsymbol{v}_b^l + \boldsymbol{g}^l \\ \boldsymbol{C}_{b2l}\left(\boldsymbol{\Omega}^b - \boldsymbol{\Omega}_{il}^b\right) \end{bmatrix} \quad \textbf{(16)}$$

where $\boldsymbol{g}^l$ is the local gravity including the Gravitation term and the centripetal term related to Earth rotation.

To linearize the mechanization equation and derive the linear INS model, **Eq.(3-4)** and **Eq.(9-11)** are applied to the mechanization equation using the perturbation analysis described in [2]. Based on this analysis, The INS state transition matrix $\boldsymbol{F}_{INS}$ and the design matrix $\boldsymbol{G}_{INS}$ are derived in the (l) frame. Their expressions are given in our previous paper [13].

We model the inertial measurement bias and scale factor errors as Gauss-Markov process [12]:

$$\delta \dot{e}_{su} = -\frac{1}{\tau_{e_{su}}} \cdot \delta e_{su} + \eta_{e_{su}} \quad \textbf{(17)}$$

where e is the error ($e = b$ or $e = k$), s is the sensor ($s = a$ or $s = g$) and u is the (b) frame axis ($u = x$, $u = y$ or $u = z$). $\tau_{e_{su}}$is the correlation time of the error e of the sensor s along the u-axis and $\eta_{e_{su}}$ is a zero-mean Gaussian noise.

The WSS scale factor as well as the GNSS clock bias and clock drift are modeled as follows:

$$\delta\left(c\dot{\delta} t_0\right) = \delta(c\delta t_0) + \eta_{\text{bias}} \quad \textbf{(18)}$$

$$\delta\left(c\ddot{\delta} t_0\right) = \eta_{\text{drift}} \quad \textbf{(19)}$$

The clock error spectral densities can be computed as:

$$q_{\text{bias}} = c^2 \cdot \frac{h_0}{2} \quad \textbf{(20)}$$

$$q_{\text{drift}} = c^2 . 2\pi^2 . h_{-2} \quad \textbf{(21)}$$

where h_0 and h_{-2} are allan variance parameters describing the clock errors, typical values for compensated crystal clock can be $2 . 10^{-19}$ and $2 . 10^{-20}$ respectively [14].

The WSS scale factor error is modeled as a constant, thus:

$$\delta \dot{k}_w = \eta_{kw} \quad \textbf{(22)}$$

The models defined previously can be summarized in the following linearized continuous time sate transition model:

$$\delta \dot{\boldsymbol{x}} = \boldsymbol{F} \cdot \delta \boldsymbol{x} + \boldsymbol{G} \cdot \boldsymbol{u} \quad \textbf{(23)}$$

where

$$\boldsymbol{F} = \begin{bmatrix} \boldsymbol{F_{INS}} & \boldsymbol{0}_{21x1} & \boldsymbol{0}_{21x1} & \boldsymbol{0}_{21x1} \\ \boldsymbol{0}_{1x21} & 0 & 1 & 0 \\ \boldsymbol{0}_{2x21} & \boldsymbol{0}_{2x1} & \boldsymbol{0}_{2x1} & \boldsymbol{0}_{2x1} \end{bmatrix} \quad \textbf{(24)}$$

$$\boldsymbol{G} = \begin{bmatrix} \boldsymbol{G}_{INS} & \boldsymbol{0}_{21x3} \\ \boldsymbol{0}_{3x21} & \boldsymbol{I}_3 \end{bmatrix} \quad \textbf{(25)}$$

$$\boldsymbol{u} = [\boldsymbol{\eta}_a \ \boldsymbol{\eta}_g \ \boldsymbol{\eta}_{ba} \ \boldsymbol{\eta}_{bg} \ \boldsymbol{\eta}_{ka} \ \boldsymbol{\eta}_{kg} \ \eta_{\text{bias}} \ \boldsymbol{\eta}_{\text{drift}} \ \eta_{kw}]^T \quad \textbf{(26)}$$

The corresponding process noise covariance matrix is given by:

$$\boldsymbol{Q} = \mathrm{cov}(\boldsymbol{u}) \quad \textbf{(27)}$$

The discrete time sate transition model assuming that $\boldsymbol{F}$ and $\boldsymbol{G}$ are constant over the time step between two consecutive state propagations Δt is given by:

$$\delta \boldsymbol{x}_{k+1} = \boldsymbol{\Phi}_k \cdot \delta \boldsymbol{x}_{k+1} + \boldsymbol{w}_k \quad \textbf{(28)}$$

with [2]

$$\boldsymbol{\Phi}_k = \boldsymbol{I} + \boldsymbol{F}.\Delta t \quad \textbf{(29)}$$

and

$$\mathbf{Q}_k = \mathrm{cov}(\boldsymbol{w}_k) = \boldsymbol{\Phi}_k \boldsymbol{G}\boldsymbol{Q}\boldsymbol{G}^{\boldsymbol{T}}\boldsymbol{\Phi}_k^T \, \Delta t \quad \textbf{(30)}$$

With the discrete state transition model, we can propagate the state using the prediction equations of the EKF. Since we are in a closed-loop configuration where the errors estimated by the EKF are fed back after the measurement update, the state vector should be reset to zero. Nonetheless, the state covariance is predicted using:

$$\boldsymbol{P}_{k+1}^{-} = \boldsymbol{\Phi}_k \boldsymbol{P}_k \boldsymbol{\Phi}_k^T + \mathbf{Q}_k \quad \textbf{(31)}$$

Kalman filter update

The update of the Kalman filter is performed by comparing the INS predicted states with the aiding measurements quantities, by relating the difference of the measured and predicted quantities to the state vector components. This update is performed as soon as a sensor measurement is available. This implies that the observation model varies according to the availability of aiding sensors.

GNSS observation model

The GNSS observation model is given by the following equation:

$$\delta \boldsymbol{z}_G = \begin{bmatrix} \tilde{\rho}_G^1 - \hat{\rho}_G^1 \\ \vdots \\ \tilde{\rho}_G^N - \hat{\rho}_G^N \\ \tilde{\dot{\rho}}_G^1 - \hat{\dot{\rho}}_G^1 \\ \vdots \\ \tilde{\dot{\rho}}_G^N - \hat{\dot{\rho}}_G^N \end{bmatrix} = \boldsymbol{H}_G \cdot \delta \boldsymbol{x} + \begin{bmatrix} \eta_{\rho G}^1 \\ \vdots \\ \eta_{\rho G}^N \\ \eta_{\dot{\rho} G}^1 \\ \vdots \\ \eta_{\dot{\rho} G}^N \end{bmatrix} \quad \textbf{(32)}$$

where

$$\boldsymbol{H}_G = \begin{bmatrix} \frac{(\boldsymbol{p}_s^1 - \hat{\boldsymbol{p}}_b^l)}{r^1} & 0_{3x3} & 0_{3x15} & 1 & 0 & 0 \\ \vdots & \vdots & \vdots & \vdots & \vdots & \vdots \\ \frac{(\boldsymbol{p}_s^N - \hat{\boldsymbol{p}}_b^l)}{r^N} & 0_{3x3} & 0_{3x15} & 1 & 0 & 0 \\ \frac{(\boldsymbol{v}_s^1 - \hat{\boldsymbol{v}}_b^l)}{r^1} + \frac{(\boldsymbol{p}_s^1 - \hat{\boldsymbol{p}}_b^l).\dot{r}^1}{(r^1)^2} & \frac{(\boldsymbol{p}_s^1 - \hat{\boldsymbol{p}}_b^l)}{r^1} & 0_{3x15} & 0 & 1 & 0 \\ \vdots & \vdots & \vdots & \vdots & \vdots & \vdots \\ \frac{(\boldsymbol{v}_s^N - \hat{\boldsymbol{v}}_b^l)}{r^N} + \frac{(\boldsymbol{p}_s^N - \hat{\boldsymbol{p}}_b^l).\dot{r}^N}{(r^N)^2} & \frac{(\boldsymbol{p}_s^N - \hat{\boldsymbol{p}}_b^l)}{r^N} & 0_{3x15} & 0 & 1 & 0 \end{bmatrix} \quad \textbf{(33)}$$

$\boldsymbol{p}_s^i$ and $\boldsymbol{v}_s^i$ are respectively the position and the velocity of satellite *i* computed in (*l*) frame.

WSS and NHC observation model:

$$\begin{aligned} \delta \boldsymbol{z}_w &= \tilde{\boldsymbol{v}}_w^l - \boldsymbol{C}_{b2l}\boldsymbol{\Omega}_{lb}^b \Delta \boldsymbol{p}_w^b - \hat{\boldsymbol{v}}_b^l \\ &= \boldsymbol{H}_w \cdot \delta \boldsymbol{x} + \boldsymbol{\eta}_w \end{aligned} \quad \textbf{(34)}$$

with [15]:

$$\boldsymbol{H}_w = [\mathbf{0}_3 \mid \; -\boldsymbol{I}_3 \mid \; (\hat{\boldsymbol{v}}_b^l)\times \mid \; \mathbf{0}_3 \mid \; \widehat{\boldsymbol{C}}_{b2l}(\Delta \boldsymbol{p}_w^b)\times \mid \; \mathbf{0}_{3x8} \mid \; (\hat{\boldsymbol{v}}_b^l + \widehat{\boldsymbol{C}}_{b2l}\boldsymbol{\Omega}_{lb}^b \Delta \boldsymbol{p}_w^b)] \quad \textbf{(35)}$$

and

- $\boldsymbol{\Omega}_{lb}^b = (\tilde{\boldsymbol{\Omega}}^{\mathrm{b}} - \boldsymbol{\Omega}_{il}^b)$, $\boldsymbol{\Omega}^{\mathrm{b}}$ and $\boldsymbol{\Omega}_{il}^b$ are respectively the skew-symmetric matrix of the gyro measurement $\tilde{\omega}^b$and of ω_{il}^b.
- $\boldsymbol{\omega}_{il}^b = \boldsymbol{C}_{b2l}^T(\boldsymbol{\omega}_{ie}^l + \boldsymbol{\omega}_{el}^l)$, with $\boldsymbol{\omega}_{ie}^l$ is the earth rate and $\boldsymbol{\omega}_{el}^l$ is the transport rate resolved in (l) frame.

where the notation $(\boldsymbol{a})\times$ means the skew-symmetric matrix of the $(3x3)$ vector $\boldsymbol{a}$.

ZVU observation model

The update based on ZVU is derived from the previous equations as follows:

$$\delta \boldsymbol{z}_{ZVU} = -\hat{\boldsymbol{v}}_b^l = \boldsymbol{H}_{ZVU}\delta \boldsymbol{x} + \boldsymbol{\eta}_{ZVU} \quad \textbf{(36)}$$

with

$$\boldsymbol{H}_{ZVU} = [\mathbf{0}_3 \quad -\boldsymbol{I}_3 \quad \mathbf{0}_{3x18}] \quad \textbf{(37)}$$

Vision observation model

The heading observation is related to the state vector by the following equation:

$$\delta z_\psi = \tilde{\psi}_{VSLAM}^l - \hat{\psi}_{INS}^l = \boldsymbol{H}_\psi \delta \boldsymbol{x} + \eta_\psi \quad \textbf{(38)}$$

with

$$\boldsymbol{H}_\psi = \begin{bmatrix} 0_{1x6} & \frac{-\hat{C}_{b2l}^{12}\hat{C}_{b2l}^{32}}{[\hat{C}_{b2l}^{12}]^2 + [\hat{C}_{b2l}^{22}]^2} & \frac{-\hat{C}_{b2l}^{22}\hat{C}_{b2l}^{32}}{[\hat{C}_{b2l}^{12}]^2 + [\hat{C}_{b2l}^{22}]^2} & 1 & 0_{1x17} \end{bmatrix} \quad \textbf{(39)}$$

ZARU observation model

Based on **Eq. 4**, when the vehicle is stationary or moves in linear motion, the actual angular rate is equal to zero. This means that the measurements given by the IMU gyroscopes are equal to the gyro biases:

$$\delta \boldsymbol{z}_{ZARU} = \tilde{\boldsymbol{\omega}}^b = \boldsymbol{b}_g + \boldsymbol{\eta}_g = \boldsymbol{H}_{ZARU}\delta \boldsymbol{x} + \boldsymbol{\eta}_g \quad \textbf{(40)}$$

with

$$\boldsymbol{H}_{ZARU} = [0_{3x12} \quad \boldsymbol{I}_3 \quad 0_{3x9}] \quad \textbf{(41)}$$

Kalman filter update

Once $\delta \boldsymbol{z}$ and $\boldsymbol{H}$ are determined, the update is performed using the Kalman filter equations:

$$\boldsymbol{K}_{k+1} = \boldsymbol{P}_{k+1}^{-}\boldsymbol{H}_{k+1}{}^{T} \cdot \left[\boldsymbol{H}_{k+1}\boldsymbol{P}_{k+1}^{-}\boldsymbol{H}_{k+1}{}^{T} + \boldsymbol{R}_{k+1}\right]^{-1} \quad (42)$$

$$\delta \hat{\boldsymbol{x}}_{k+1}^{+} = \boldsymbol{K}_{k+1}\delta \boldsymbol{z}_{k} \quad (43)$$

$$\boldsymbol{P}_{k+1}^{+} = \boldsymbol{P}_{k+1}^{-} - \boldsymbol{K}_{k+1} \cdot \boldsymbol{H}_{k+1} \cdot \boldsymbol{P}_{k+1}^{-} \quad (44)$$

where $\boldsymbol{R}$ is the measurement covariance matrix.

EXPERIMENTS AND RESULTS

The algorithm is tested using GNSS and inertial data collected in Toulouse downtown during 30 minutes. GNSS data is given by the GPS L1 C/A stand-alone mode of a Ublox-6 receiver running at **1Hz**. Inertial measurements are obtained using an Xsens Mti IMU running at **100 Hz. Figure 3** shows the reference trajectory determined using the NovAtel SPAN equipment [16].

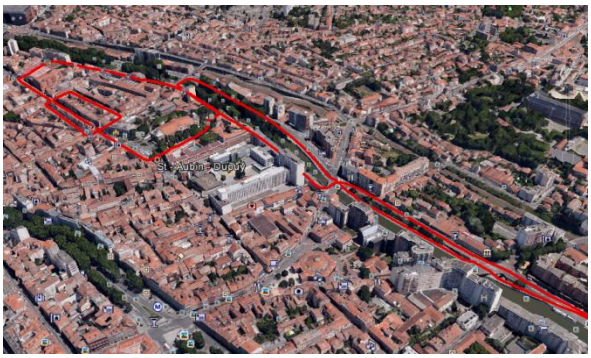

Figure 3: Vehicle trajectory in Toulouse downtown

The WSS velocity and visual data are generated from the reference trajectory such that the WSS is affected by a scale factor of ***-0.01*** and a zero-mean white Gaussian noise with a standard deviation equal to ***0.05m/s***. The SLAM heading is assumed to be a zero-mean white Gaussian noise with a standard deviation of ***2°***. The WSS and SLAM are assumed to run respectively at ***10Hz*** and ***20 Hz***. As mentioned before, only the horizontal performance will be assessed in this study.

To evaluate the contribution of each aiding sensor, seven configurations are tested and compared in this study. A GPS outage of 60s is also simulated in order to assess the performance of the DR system during GPS outage:

- Config1: GNSS
- Config2: GNSS+INS
- Config3: GNSS+INS+Innovation test
- Config4: Config3+NHC+ZVU+ZARU
- Config5: Config4+WSS
- Config6: Config5+heading
- Config7: DR sensor

Config1 results

In this configuration we assume that the positioning is only based on GPS L1 C/A signals. As illustrated in **Figure 4**, the horizontal error is very important especially when the vehicle goes through dense streets (between 550s and 700s). In this environment, the horizontal error reaches **172m**. In addition, when less than 4 satellites are in view, GPS is unable to provide a navigation solution.

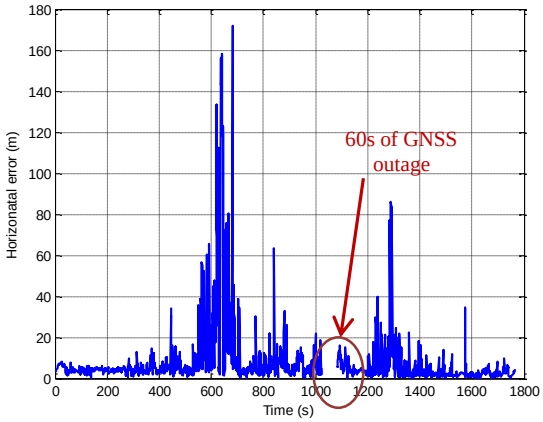

Figure 4: Stand-alone GPS horizontal position error

Config2 results

This configuration consists of an INS based on the Xsens IMU measurements corrected by the pseudo-range and Doppler measurements from GPS in a closed-loop tight configuration. No aiding comes from any of the other sensors. During GPS outage, the system is able to coast thanks to the continuity of the inertial sensor. As illustrated in **Figure 5**, the position accuracy is increased when GPS is available and there is no discontinuity anymore. For example, between 550s and 770s, the RMSE is decreased by **87.1%**. Yet the horizontal error remains very high especially during GPS outage. An error of **805m** is reached after 60s of outage.

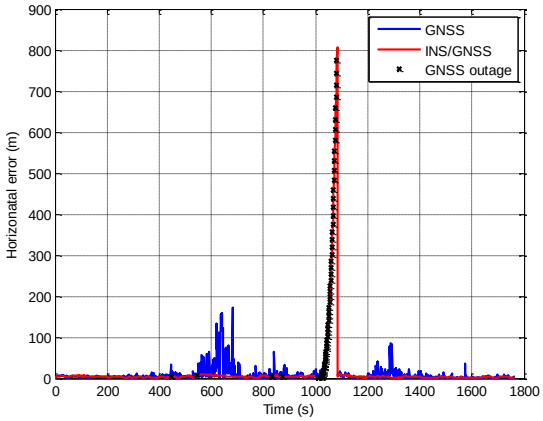

Figure 5: Comparison of horizontal position error

Config3 results

This configuration adds the innovation test of GPS measurements before using them to update the Kalman state vector. This innovation test is very important in order to improve the navigation solution in urban environments when GPS measurements are available by eliminating the erroneous measurements. In fact, by removing the measurements inconsistent with previous information, we only keep the measurements that are not

affected by large error. **Figure 6** shows the number of excluded pseudo-ranges and pseudo-range rates at each epoch.

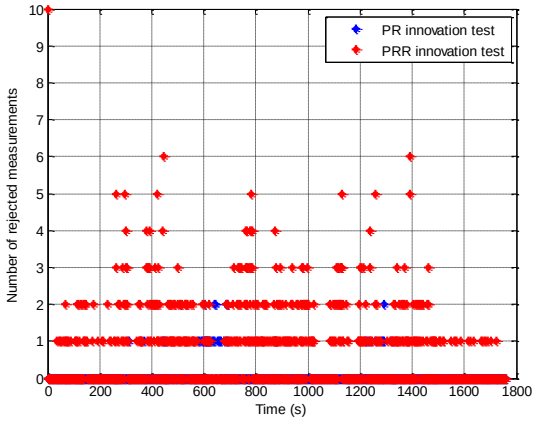

Figure 6: Number of removed SVs with innovation test

It is important to check that after exclusion, the number of remaining satellites keeps high enough to improve the navigation solution. A drawback of this technique is that in case of little number of remaining satellites, the performance may be degraded due to the exclusion. In our case, the remaining number of measurements is high enough to be able to exclude without degrading the performance. **Table 2** gives the availability of satellites during the measurement campaign (The simulated GPS outage is not considered):

Number of SVs	Pseudo-range test	Pseudo-range rate test
0 < N < 2	0 %	0.2 %
2 ≤ N < 4	0.3 %	2.6 %
4 ≤ N < 6	12.7 %	20.5 %
6 ≤ N < 8	39 %	40.4 %
≥ 8	48%	36.4 %

Table 2: Satellite availability after exclusion

Figure 7 and **Figure 8** highlight the contribution of this technique in the improvement of the navigation solution when GPS measurements are available (without simulating the GPS outage of 60s).

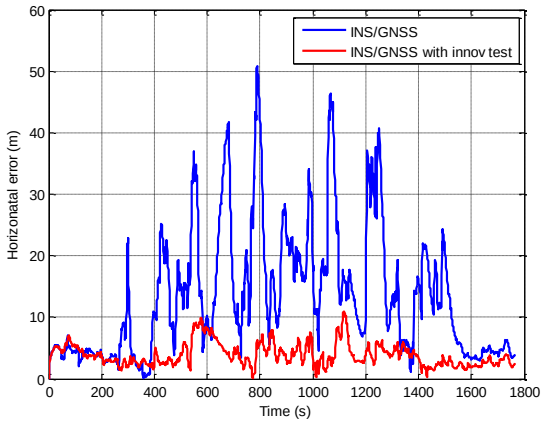

Figure 7: Comparison of horizontal position error

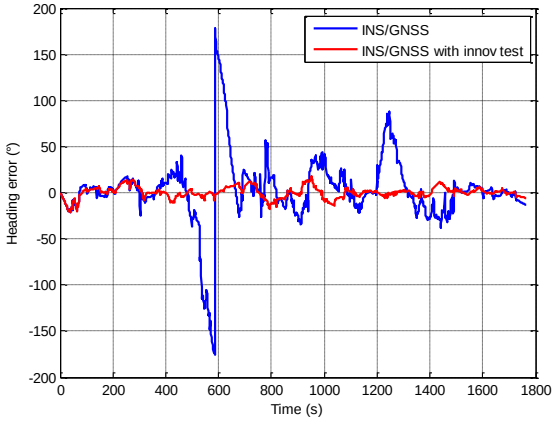

Figure 8: Comparison of heading error with and without innovation test

As explained before, the fact that after exclusion, the number of the remaining good measurements is high helps to improve the navigation solution. The RMSE is decreased by **75.24%** after applying the innovation test.

Config4 results

This configuration adds constraints related to the vehicle motion. The advantage of adding these constraints is that it does not have an additional cost compared to the previous configuration. The comparison of the horizontal error made using this configuration and that using the previous configuration shows that the estimation is clearly improved by introducing these constraints as shown in **Figure 9** and **Figure 11**. However, in GPS outage, the drift of the navigation solution remains unacceptable since it reaches **309m** after 60s of outage.

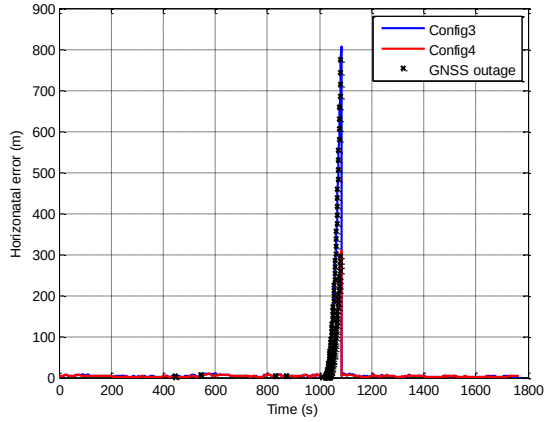

Figure 9: Comparison of horizontal position error

When GPS is available, the use of motion constraints improves slightly the performance of the navigation solution. This is highlighted in **Figure 10.**

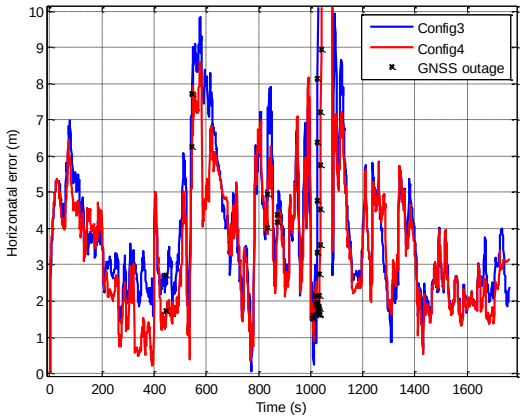

Figure 10: Comparison of horizontal position error when GPS is available

In **Figure 11**, the heading estimation is clearly improved by using the motion constraints. This is due to 2 main reasons: first, the ZARU allows the improvement of attitude estimation by helping estimating the gyro biases. In addition, the ZVU and NHC improve the velocity estimation. This is due to the correlation that exists between the vehicle velocity and its attitude.

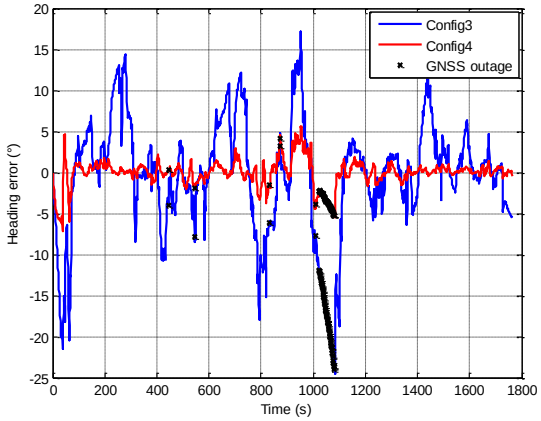

Figure 11: Comparison of heading error

Config5 results

In this configuration, the WSS is added. This sensor provides additional information to the filter about its longitudinal velocity. The comparison of the navigation performance with the previous configuration shows that the horizontal position error is improved as shown in **Figure 12**. The drift during GPS outage is reduced from **309m** to about **19.5m** which is an improvement of **93.7%.** When GPS is available and the innovation test on GPS measurements is performed, we have almost the same navigation performance as the previous configuration**.**

For the heading, no improvement is noticed compared to the previous configuration as shown in **Figure 13.**

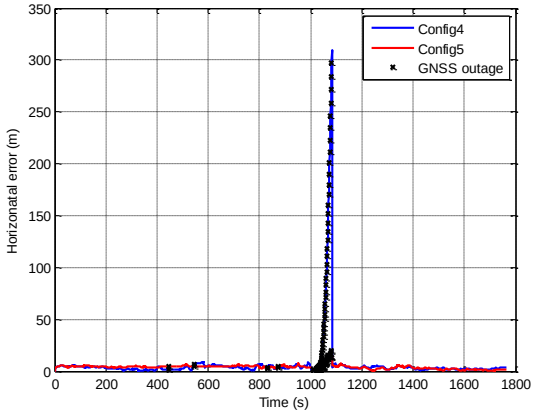

Figure 12: Comparison of horizontal position error

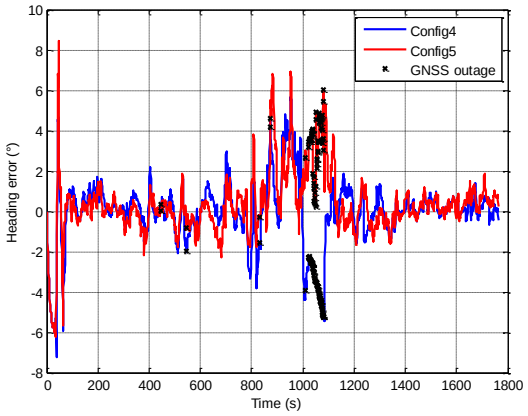

Figure 13: Comparison of heading error

Config6 results

In this configuration, the SLAM heading is added. As mentioned before, this heading is assumed as a zero-mean white Gaussian noise. This assumption could be realistic if the vehicle finishes its trajectory at its starting point, or if we have a previously built georeferenced database. The results introducing this information show an important improvement of the heading estimation as shown in **Figure 14.**

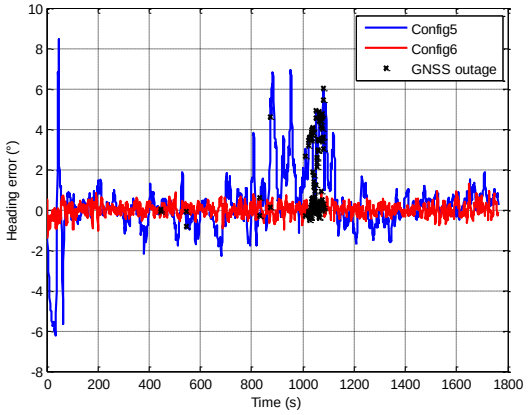

Figure 14: Comparison of heading error

For the horizontal error, this information is quite important since it reduces the drift of the DR system when

GPS is unavailable and reduces the horizontal error when GPS is available, as illustrated in **Figure 15**. During the 60s of GPS outage, the error does not exceed **1.2m** when we introduce the heading information.

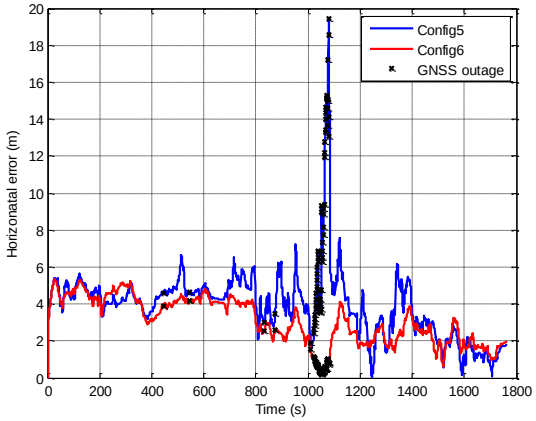

Figure 15: Comparison of horizontal position error

Config7 results

This configuration is tested in order to analyze the possible drift of the DR system without the use of GPS aid during the full trajectory. **Figure 16** shows that the DR system is able to provide a navigation solution without drift. It also shows that the performance of the DR system with GPS aid is slightly better.

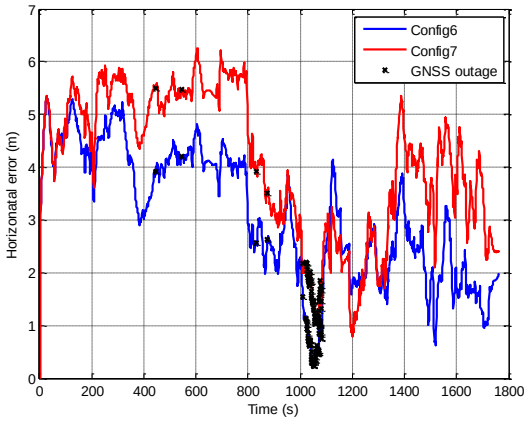

Figure 16: Comparison of heading error

Summary

Table 3 summarizes the performance of the different tested configurations. It compares the errors of horizontal position and heading in terms of the maximum reached error and in terms of Root Mean Square (RMS). This summary shows the limitations of using a simple GNSS/INS integration in urban environment and highlights the contribution of each sensor in the improvement of the horizontal navigation solution.

param / Config	Horizontal position error (m)		Heading error (°)	
	Max	RMS	Max	RMS
1	172	33	---	---
2	805	> 100	> 100	
3	805	64.62	17.22	7
4	309	23,52	5.65	1.6
5	19.45	4.36	8.46	1.59
6	5.34	3.34	1.31	0.31
7	6.25	4.3	0.89	0.28

Table 3: Comparison of the different configurations

CONCLUSION

In this paper, we proposed an algorithm integrating different low-cost sensors in order to improve the navigation performance in terms of accuracy and continuity in urban environments. This algorithm fuses information from an IMU considered as the reference sensor which is aided by GNSS raw measurements, WSS velocity, SLAM heading and motion constraints. Results show that the use of a GNSS/INS system is not sufficient especially in urban environments where the GNSS measurements could be corrupted or unavailable. GNSS outage was simulated to evaluate the horizontal positioning and heading drift by comparing 7 configurations. This comparison aimed to highlight the contribution of each additional sensor to the decrease of the drift when GNSS is unavailable and to the improvement of the navigation solution when GNSS measurements are corrupted. A horizontal error RMS of **3.34m** on a trajectory of 30 minutes is achieved. This was possible thanks to the good SLAM heading considered in this study. However, this assumption is not realistic if the SLAM algorithm relies only on the DR principle. Future works should focus on the improvement of the SLAM measurement model and on the accuracy improvement of the navigation solution since the performance required by the project is still not achieved.

REFERENCES

[1] Z. Jiang, P.D. Groves: "NLOS GPS signal detection using a dual polarisation antenna", GPS Solutions, pp. 1–12, 2012

[2] E.H. Shin: "Accuracy improvement of low cost INS/GPS for land applications", PhD Thesis, Department of Geomatics Engineering, University of Calgary, 2001

[3] M. Spangenberg, V. Calmettes, D. Kubrak, and O. Julien, “Optimized low-cost HSGPS/IMU/WSS land vehicle navigation system for urban navigation,” in Proceedings of the 20th International Technical Meeting of the Satellite Division of the Institute of Navigation (ION GNSS '07), pp. 70–78, U.S. Institute of Navigation, Fort Worth Tex, USA, September 2007

[4] D. Nistér,O. Naroditsky, J. Bergen: "Visual odometry for ground vehicle applications", Journal of Field Robotics, 2006, 23, (1), pp.3-20

[5] S. Hong, J.B. Song, J.H. Baek, J.K. Ryu.: "Visual odometry for outdoor environment using a downward-tilting camera and self-shadow removal algorithm", Proc. IEEE Int. Conf. Control, Automation and Systems (ICCAS), 2012, pp.960-963

[6] G. Nutzi, S. Weiss, D. Scaramuzza and R. Siegwart: "Fusion of IMU and vision for absolute scale estimation in monocular SLAM", Journal of Intelligent and Robotic Systems, **61**(1–4), 287–299

[7] A. Ben-Afia, L.Deambrogio, D. Salos, et al: "Review and classification of vision-based localisation techniques in unknown environment" , IET Radar, Sonar & Navigation, Volume 8, Issue 9, December 2014, p. 1059 – 1072

[8] C. Engles, H. Stewénius, D. Nistér: "Bundle adjustment rules", Proc. Symp. Photogrammetric Computer Vision, 2006

[9] G. Dissanayake, S. Sukkarieh , E. Nebot and H. Durrant-Whyte: "The aiding of a low-cost strapdown inertial measurement unit using vehicle model constraints for land vehicle applications", IEEE Trans.Robot. Autom., vol. 17, no. 5, pp.731 -747, 2001

[10] P. D. Groves: "Principles of GNSS, Inertial and Multisensor Integrated Navigation Systems", Artech House, 2013

[11] A. Eudes: "Localisation et cartographie simultanées par ajustement de faisceaux local : propagation d'erreurs et réduction de la dérive à l'aide d'un odomètre", PhD thesis, University of Blaise Pascal - Clermont-Ferrand II , 2011

[12] A. Angrisano: "GNSS/INS Integration Methods", PhD thesis, University of Naples Parthenope, 2010

[13] A. Ben-Afia, A.C. Escher, C. Macabiau, S. Roche: "A GNSS/IMU/WSS/VSLAM Hybridization Using an Extended Kalman Filter", *Proceedings of the ION 2015 Pacific PNT Meeting*, Honolulu, Hawaii, April 2015, pp. 719-732

[14] R.G. Brown and P.Y.C. Hwang: "Introduction to Random Signals and Applied Kalman Filtering", John Wiley & Sons, 1997

[15] l Seo, J, Lee, H.K., Lee, J.G and Park, C.G., (2006), "Lever Arm Compensation for GPS/INS/Odometer Integrated System", Inter. Journal of Contr., Automat. and Systems, vol. 4, no. 2, pp. 247-254

[16] http://www.novatel.com/assets/Documents/Manuals/om-20000139.pdf